

# Implementation of a new magnetizing branch in EMTP-RV using the A(x) model

M. Lambert, J. Mahseredjian, L.-A. Dessaint, A. Gaudreau

**Abstract**—This paper presents a new model to describe the saturation and hysteresis effects of the magnetizing branch in a transformer. The implementation of this model is done in the EMTP-RV environment. The A(x) model will be first explained and the details regarding its implementation will be discussed. Afterwards, the results of this model are compared to other existing models. The A(x) model can account for a wide range of hysteresis shapes. It is also computationally efficient and only the major loop data is needed to fully describe the trajectories. Furthermore, the A(x) model is capable of modeling the wider part of the major loop near saturation, where most models tend to fail.

**Keywords:** hysteresis, saturation, transformer, electromagnetic transients, EMTP.

## I. INTRODUCTION

NUMEROUS models of hysteresis and saturation have been developed throughout the years, all of which have advantages and disadvantages. Some of them are fundamental in nature and attempt to explain the nanoscopic behavior of the magnetic media, while others are phenomenological and simply rely on experimental data and mathematical functions. Hysteresis and saturation are often confounded with each another. The hysteresis phenomenon is based on the branching due to the excitation's history that can eventually lead to the formation of loops, while saturation results in the inability of the response to further raise to an increase in excitation [1]. It is a thermodynamic process in which losses are produced and in which case the generated trajectory in the  $B(H)$  plane will be counterclockwise [2]. While both phenomena can be represented separately, the model proposed in this paper attempts to model both using a unique branch that will be referred to as the magnetizing branch.

---

This work was supported in part by the TransÉnergie Chair on Simulation and Control of Electric Power Systems

M. Lambert and J. Mahseredjian are with the Department of Electrical Engineering, École Polytechnique de Montréal, Montréal, QC H3T 1J4, Canada (e-mail: jeanm@polymtl.ca).

L.-A. Dessaint is with the Department of Electrical Engineering, École de technologie supérieure, Montréal, QC H3C 1K3, Canada.

A. Gaudreau is with the IREQ, Hydro-Québec's Research Institute, Varennes, QC J3X 1S1, Canada.

Paper submitted to the International Conference on Power Systems Transients (IPST2009) in Kyoto, Japan June 3-6, 2009

Phenomenological models are normally based on hyperbolic functions to mimic nonlinear behavior [3][4][5]. These functions are asymptotic in nature, just like the saturation phenomenon and the hysteresis effect can be accounted for with a simple translation. These models rely on nonlinear regression techniques and the quality of the fit to the experimental major loop data depends on the number of degrees of freedom of the mathematical model. In particular, the thicker part of the loop near saturation is often the source of fitting inaccuracies, as it can be seen in [6] and [7]. Moreover, this gooseneck appearance is often attributed to eddy currents, but it has been shown otherwise in [7]. In order to account for this phenomenon and produce more accurate regressions, a new model is required.

First, there are a few prerequisites to choose the right function. Because of saturation, the model needs to be asymptotic and also requires a certain amount of shift, in order to account for both coercivity and remanence. Furthermore, it has to reproduce the gooseneck appearance of the curve, which means that the function is asymmetrical with respect to the abscissa and the ordinate. In other words, the lower part of the upward branch is not a 180 degrees rotation of the upper part. Also, the model needs to account for the reversible part of magnetization and should have enough degrees of freedom to produce a good regression. Therefore, by combining all these requirements, a new model was created, namely the A(x) model, which is inspired from the works of [8] and [9]. It is intended for the simulation of electromagnetic transients in power systems with the goal of achieving accuracy while staying computationally efficient and it was implemented in EMTP-RV [10].

## II. THE A(x) MODEL

In order to reproduce the experimental results in phenomenological models, a function, or combination of functions need to be found, from which it will be possible to get the best regression. For this purpose, the hyperbolic tangent and the hyperbolic secant functions proved from their respective shapes, to resemble classic major loop curves exhibiting gooseneck appearances, like the one shown in Fig. 1. Let us define

$$f_1(x) = k_1 \tanh(k_2x - k_3) \quad (1)$$

$$f_2(x) = k_4 \operatorname{sech}^2(k_2x - k_3) \quad (2)$$

where parameters  $k_1$  and  $k_4$  define the amplitude, parameter  $k_3$  defines the horizontal shift and parameter  $k_2$  represents the horizontal scale of these functions. Also, the hyperbolic secant

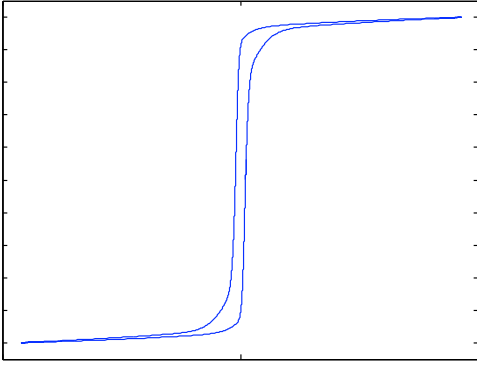


Fig. 1. Typical major loop exhibiting a gooseneck appearance

is squared in order to get a thinner curve. The behavior of these functions can be seen in Fig. 2 and 3. By shifting horizontally, the hyperbolic tangent can get the right coercivity. Although, with this function alone, the upper part is the same as the lower part and no gooseneck appearance is generated. In order to get the right curvature and differentiate the two parts, the hyperbolic secant is added to the hyperbolic tangent. At last, in order to account for a wide variety of curves and to give more leverage for better nonlinear regressions, a few more of these functions can be added to the model's function, as needed. After performing several fitting cases, it was found that the optimal number of hyperbolic tangents and hyperbolic secants was three. The  $A(x)$  function for the upward part of the major loop is given by

$$\begin{aligned}
 A(x) = & k_1 \tanh(k_2x - k_3) - k_1k_4 \text{sech}^2(k_2x - k_3) \\
 & + k_5 \tanh(k_6x - k_7) - k_5k_8 \text{sech}^2(k_6x - k_7) \\
 & + k_9 \tanh(k_{10}x - k_{11}) - k_9k_{12} \text{sech}^2(k_{10}x - k_{11}) \\
 & + k_{13}x
 \end{aligned} \quad (3)$$

where the constants  $k_1$  to  $k_{13}$  are found with the upward trajectory of the major loop, by using a nonlinear regression technique on the experimental data. The coercivity and remanence of the loop are given by the even functions, the hyperbolic secants, and by the shifting parameters  $k_3$ ,  $k_7$  and  $k_{11}$ . To generate the downward trajectory, it is simply needed to change the signs of these parameters. Also, the reversible part of magnetization can be accounted for with the addition of the linear term  $k_{13}$ . Without this term, the major loop saturates at  $A_{sat} = k_1 + k_5 + k_9$ .

Generally, the magnetization characteristic is given in terms of flux density as a function of magnetic field intensity  $B(H)$ . However, it is more convenient to work with flux linkage and current from an EMTP perspective, since these can be easily measured experimentally and compared to simulation, regardless of the transformer's configuration. To obtain the flux linkage, it is simply needed to integrate the voltage. Translating (3) in terms of flux linkage and current gives

$$\begin{aligned}
 \Psi_+(i) = & k_1 \tanh(k_2i - k_3) - k_1k_4 \text{sech}^2(k_2i - k_3) \\
 & + k_5 \tanh(k_6i - k_7) - k_5k_8 \text{sech}^2(k_6i - k_7) \\
 & + k_9 \tanh(k_{10}i - k_{11}) - k_9k_{12} \text{sech}^2(k_{10}i - k_{11}) \\
 & + k_{13}i
 \end{aligned} \quad (4)$$

for the upward trajectory of the major loop and

$$\begin{aligned}
 \Psi_-(i) = & k_1 \tanh(k_2i + k_3) + k_1k_4 \text{sech}^2(k_2i + k_3) \\
 & + k_5 \tanh(k_6i + k_7) + k_5k_8 \text{sech}^2(k_6i + k_7) \\
 & + k_9 \tanh(k_{10}i + k_{11}) + k_9k_{12} \text{sech}^2(k_{10}i + k_{11}) \\
 & + k_{13}i
 \end{aligned} \quad (5)$$

for the downward part.

To define the minor loops, one must recall that all trajectories must remain inside the major loop. In order to do so, the major loop must be only reached at infinite excitation. This axiom constitutes the asymptotic behavior for all trajectories. Also, at the current reversal point  $i_{r_n}$ , the flux linkage of the upward trajectory must be equal to the flux linkage of the downward trajectory. To meet this condition, the major loop trajectories must be shifted in order to intersect at  $(i_{r_n}, \psi_{r_n})$ . The shifting parameter must equate the two flux linkages at reversal and gradually nullify when approaching saturation. From these considerations, we derive the general equations for the model

$$\psi_+(i) = \Psi_+(i) + C_{n+}(i) \quad (6)$$

$$\psi_-(i) = \Psi_-(i) + C_{n-}(i) \quad (7)$$

where  $C_{n+}(i)$  and  $C_{n-}(i)$  are the parameters that modify the upward and downward major loop trajectories, respectively. These parameters are given by

$$\begin{aligned}
 C_{n+}(i) = & C_{nu+} \left( \frac{a_+(i_{r_{n-1}}) - a_+(i)}{a_+(i_{r_{n-1}}) - a_+(i_{r_n})} \right) \\
 & + C_{nd+} \left( \frac{a_+(i_{r_n}) - a_+(i)}{a_+(i_{r_n}) - a_+(i_{r_{n-1}})} \right)
 \end{aligned} \quad (8)$$

$$\begin{aligned}
 C_{n-}(i) = & C_{nu-} \left( \frac{a_-(i_{r_{n-1}}) - a_-(i)}{a_-(i_{r_{n-1}}) - a_-(i_{r_n})} \right) \\
 & + C_{nd-} \left( \frac{a_-(i_{r_n}) - a_-(i)}{a_-(i_{r_n}) - a_-(i_{r_{n-1}})} \right)
 \end{aligned} \quad (9)$$

where the subscript  $n$  denotes the order of reversal. At the point of reversal, we have  $C_n(i) = C_{nu}$ , because of the leverage provided by the functions  $a(i)$ . So, the constants  $C_{nu+}$  and  $C_{nu-}$  are the differences in flux linkage between the reversal point and the major loop.

Another axiom for this model is the deletion of past input extrema if the excitation is increased in amplitude beyond intermediate extrema. This property highlights the need to keep a list of all the reversal points. If the excitation is monotonically increased beyond the last maximum, it shall be deleted, along with the last minimum. Same situation applies when the excitation is monotonically decreased further than the last minimum. Also, in this model, the minor loops must be closed, i.e. the  $n^{\text{th}}$  order reversal curve must reach  $(i_{r_{n-1}}, \psi_{r_{n-1}})$ , should the excitation be brought back to its former extrema. Referring to (8) and (9), we have  $C_n(i) = C_{nd}$  at  $i_{r_{n-1}}$  and because of the last property, the constants  $C_{nd+}$  and  $C_{nd-}$  thus become the difference in flux linkage between the  $(n-1)^{\text{th}}$  reversal point and the major loop.

To illustrate the working principle of the minor loop trajectories, a third order reversal curve is shown in Fig. 4. There

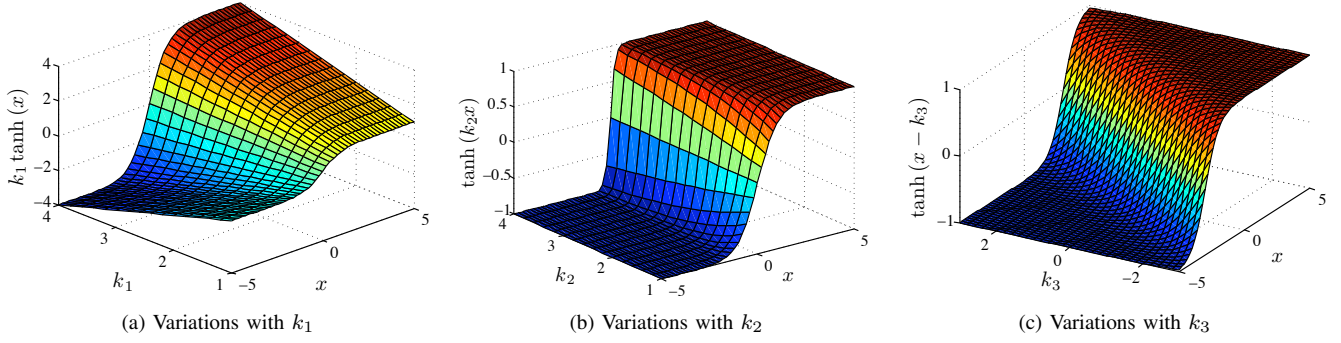


Fig. 2. The hyperbolic tangent function in relation to its parameters

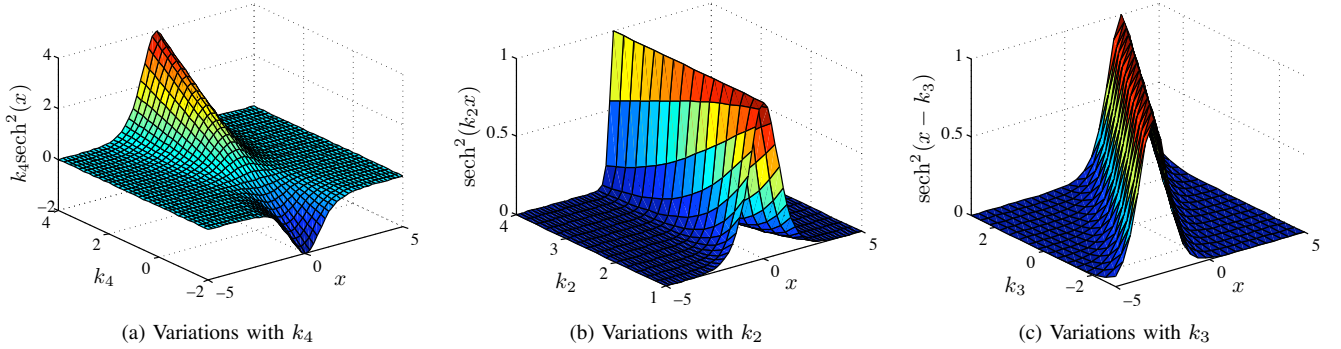


Fig. 3. The hyperbolic secant function in relation to its parameters

are three reversal points,  $(i_{r1}, \psi_{r1})$ ,  $(i_{r2}, \psi_{r2})$  and  $(i_{r3}, \psi_{r3})$ , respectively. In the downward third order reversal trajectory, the constants  $C_{3d-}$  and  $C_{3u-}$  are calculated when the third reversal is detected. Like it is illustrated, the constant  $C_{3u-}$  is the difference in flux linkage between  $\Psi_-$  and  $\psi_{r3}$  and the constant  $C_{3d-}$  is the difference in flux linkage between  $\Psi_-$  and  $\psi_{r2}$ .

On the other hand, the leverage functions  $a(i)$  must be chosen in order for the minor loops to mimic the hyperbolic nature of the major loop. After experimenting with several leverage functions, the chosen functions that reproduce this behavior are

$$a_+(i) = k_1 \tanh(k_2 i - k_3) - k_1 k_4 \text{sech}^2(k_2 i - k_3) + k_5 \tanh(k_6 i - k_7) - k_5 k_8 \text{sech}^2(k_6 i - k_7) + k_9 \tanh(k_{10} i - k_{11}) - k_9 k_{12} \text{sech}^2(k_{10} i - k_{11}) \quad (10)$$

$$a_-(i) = k_1 \tanh(k_2 i + k_3) + k_1 k_4 \text{sech}^2(k_2 i + k_3) + k_5 \tanh(k_6 i + k_7) + k_5 k_8 \text{sech}^2(k_6 i + k_7) + k_9 \tanh(k_{10} i + k_{11}) + k_9 k_{12} \text{sech}^2(k_{10} i + k_{11}) \quad (11)$$

The reversible part of magnetization has been taken out of these equations, since the leverage functions need to saturate in order to stay within the major loop.

Finally, the model also needs to represent the first magnetization process when the transformer is deenergized. In order to do so, the stack must be filled with vertices that follow the virgin magnetization curve. Because of the deletion property and of the closed loop axiom, the trajectory will follow the extrema from the stack. Hence, in order to fill the

stack with vertices, a new function is needed to generate the virgin magnetization curve

$$\psi_{virgin}(i) = (k_1 \tanh(k_2 i) + k_5 \tanh(k_6 i) + k_9 \tanh(k_{10} i) + k_{13} i)(1 - 2k_{14} \text{sech}^2(k_{15} i)) \quad (12)$$

where  $k_{14}$  is the initial curvature and is defined between zero and one half. The higher this parameter is, the more curvature there will be around origin, which in other terms results in a lower initial slope. On the other hand, the parameter  $k_{15}$  will modify the slope below saturation, which is adjusted to fit the major loop. Typically, a value of  $\max\{k_2, k_6, k_{10}\}$  will be acceptable in most cases, but it can be manually modified during fitting.

### III. NUMERICAL IMPLEMENTATION

The A(x) model was programmed in Fortran-95 as a DLL and it was interfaced with the core code of EMTP-RV by using the guidelines provided in [11]. Furthermore, the numerical implementation is based on the works of [6] and [12].

In EMTP-RV, the nonlinear devices are solved simultaneously with the linear network equations. The nonlinear devices are linearized at each time-point and replaced by their Norton equivalent for solving the complete system of network equations. A Newton iterative procedure is applied at each time point to find the right equivalent for each nonlinear device. As such, the flux linkage is considered to be the excitation and the current is the response of the magnetizing branch.

At a given time-point  $\tau$ , the iterative process starts by

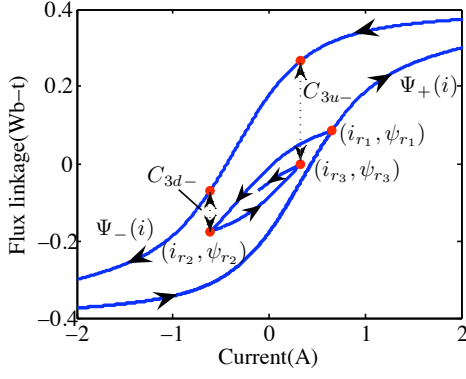


Fig. 4. Minor loop trajectories showing a third order reversal curve

calculating the flux linkage from the voltage

$$\psi_{km}(\tau) = \int_{\tau-\Delta t}^{\tau} v_{km}(\tau)dt + \psi_{km}(\tau - \Delta t) \quad (13)$$

where  $k$  and  $m$  are the connectivity nodes of the magnetizing branch,  $v_{km}$  is the voltage and  $\Delta t$  is the integration time step. Equation (13) is solved using the trapezoidal integration method. EMTP-RV also applies the Backward Euler method for discontinuity treatment. The generic solution is given by

$$\psi_{km}(\tau) = \frac{\Delta t}{2} v_{km}(\tau) + \psi_{km\text{hist}}(\tau) \quad (14)$$

where the term  $\psi_{km\text{hist}}(\tau)$  depends on the solution method. For the trapezoidal method, it is given by

$$\psi_{km\text{hist}}(\tau) = \frac{\Delta t}{2} v_{km}(\tau - \Delta t) + \psi_{km}(\tau - \Delta t) \quad (15)$$

and for the Backward Euler method

$$\psi_{km\text{hist}}(\tau) = \psi_{km}(\tau - \Delta t) \quad (16)$$

Afterwards, the branch's current  $i_{km}(\tau)$  corresponding to the flux linkage found with (14) is calculated from (6) and (7) by means of the Newton iterative method. This is because the  $A(x)$  model is given in terms of  $\psi(i)$  and there is no explicit solution to  $i(\psi)$ , namely the inverse function. After the quiescent point  $(i_{km}(\tau), \psi_{km}(\tau))$  has been found, the function can be locally linearized, assuming that the integration time step is sufficiently small

$$\psi_{km}(\tau) = K_q i_{km}(\tau) + \psi_q \quad (17)$$

where  $K_q$  is the slope and  $\psi_q$  is the ordinate at origin of the linearization. The slope can be found from

$$K_q = \frac{\psi_{km}(\tau) - \psi_{km}(\tau - \Delta t)}{i_{km}(\tau) - i_{km}(\tau - \Delta t)} \quad (18)$$

since there exists no analytic inverse function to the function  $\psi(i)$  and thus, its derivative cannot be analytically found. Then, the ordinate at origin can be found by solving (17) for  $\psi_q$ . By combining (14) and (17), the linearized current of the branch becomes

$$i_{km}(\tau) = \frac{\Delta t}{2K_q} v_{km}(\tau) + \frac{\psi_{km\text{hist}}(\tau) - \psi_q}{K_q} \quad (19)$$

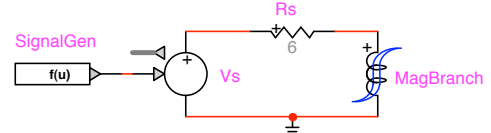


Fig. 5. Benchmark circuit 1

The iterative Norton equivalent is found directly from (19). This equivalent is in turn given back to EMTP-RV to solve the network equations and the Newton iterative process for nonlinear devices continues until all nonlinear devices have converged. As for the steady-state initialization, the linear inductance corresponding to the initial slope at coercivity is inserted into the network equations to calculate the steady-state flux linkage and the corresponding steady-state current, assuming that the initial trajectory starts on the major loop.

A few concluding remarks need to be made regarding the limitations of the  $A(x)$  model. First, this model is not frequency dependent, i.e. the rate of change of the excitation has no effect on the trajectories, only the past extrema does. It is said to be rate independent and assumes that the frequency is sufficiently high to overcome the thermal relaxation effects, while sufficiently low to neglect the eddy current variations [2]. Secondly, the high number of degrees of freedom of the  $A(x)$  function and the complexity of the major loop shape complicates the computation of the nonlinear regression. For this matter, a new curve fitter was implemented, which uses the MATLAB curve fitting toolbox [13] routines in order to find the values for parameters  $k_1$  to  $k_{13}$ , obtained from the ascending branch of the experimental major loop.

#### IV. SIMULATION BENCHMARK

In order to assess the validity of the proposed model, two benchmarks were created in EMTP-RV to simulate various minor loop trajectories. Moreover, all the parameters used for these simulations can be found in the appendix.

The first circuit consists of a controlled voltage source in series with a resistance and the magnetizing branch, as shown in Fig. 5. The resistance is inserted to allow the distortion of the voltage and thus the flux linkage of the magnetizing branch. It will be used to verify opened minor loop trajectories. To do so, the function from the signal generator is set to

$$f_g(t) = 1500t \sin(120\pi t)$$

The corresponding signal is shown in Fig. 6.

The second benchmark will test whether the model produces good fitting results or not and will be used to compare with the results of the actual EMTP-RV hysteretic reactor [7][12]. The experimental data used for the nonlinear regression is the overexcitation at 1.4 pu of the 370 MVA transformer found in [14]. The overexcitation has to be as large as possible in order to get a loop close enough to the asymptotic major loop. The corresponding circuit is shown in Fig. 7. Here, the source of 1.4 pu with a short-circuit current of 24 kA is represented by a voltage source of 177 kV<sub>(rms)</sub> and an impedance of  $(0.21 + j7.38)\Omega$ . Since the reactor's major loop will mimic the experimental  $\psi(i)$  curve at 1.4 pu overexcitation in unloaded

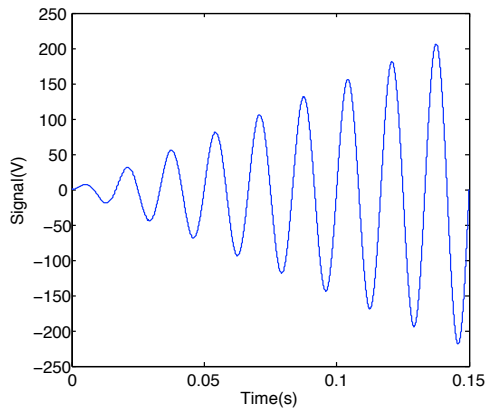


Fig. 6. Generator signal

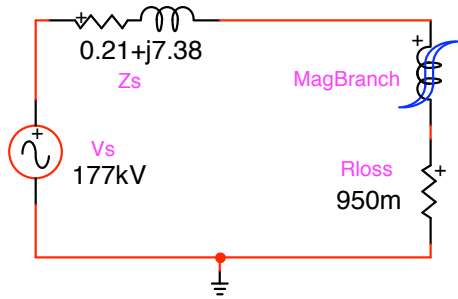


Fig. 7. Benchmark circuit 2

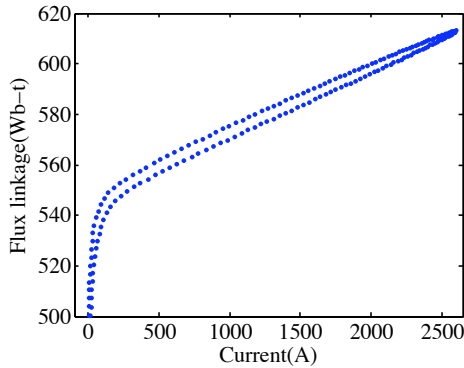


Fig. 8. Experimental data showing losses in the saturation region

conditions, there is no need to add the series and shunt impedances of the classical transformer model. Instead, only a series resistance is needed in order to account for the finite area found in the saturation region, shown in Fig. 8. The equivalent resistance found from trial and error to reproduce these losses was estimated to 950 m $\Omega$ .

## V. SIMULATION RESULTS

The result of the first benchmark circuit is shown in Fig. 9. The flux linkage at  $t = 0$  is null, because the magnetizing branch is initially demagnetized. Afterwards, the unclosed minor loops progressively increase in size as the source increases and the extrema of the  $\psi - i$  characteristic form the normal magnetization curve, i.e. the trajectory that would be followed provided that the magnetic medium is in the demagnetized state. These results are in agreement with the

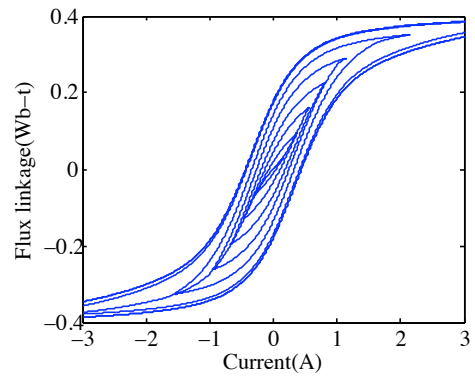


Fig. 9. Results of the first benchmark

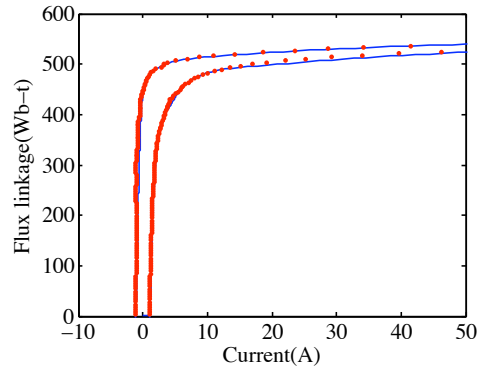


Fig. 10. Results of the second benchmark for the A(x) model

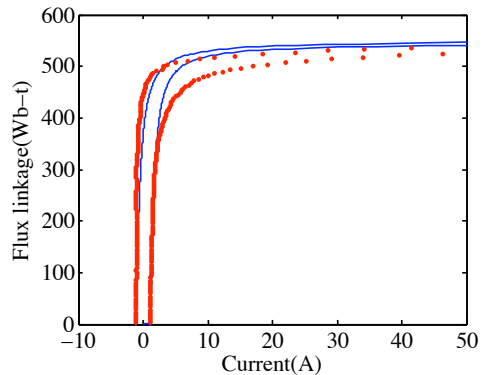


Fig. 11. Results of the second benchmark for the EMTP-RV hysteretic reactor model based on [6][7]

minor loop trajectories found in the literature [2], [8] and in turn validate the trajectories for the model.

For the second test, the results are shown in Fig. 10 to Fig. 13. Here, the experimental data is represented with dots and the simulation results are shown with a solid line. The first pair of graphs highlights the strength of the A(x) model. It is able to reproduce adequately the gooseneck appearance of the curve near saturation. Although the fitting method used in EMTP-RV is sufficiently accurate in most cases, it is limited as compared to the A(x) model fitting. In this particular case, it is unable to reproduce the wider region near saturation. This means that the losses are not modeled accurately and will affect the precision of the transient response of the magnetizing branch. Basically, models such as [7] and [15] will fail to model this part correctly because of the hypothesis that the curves are

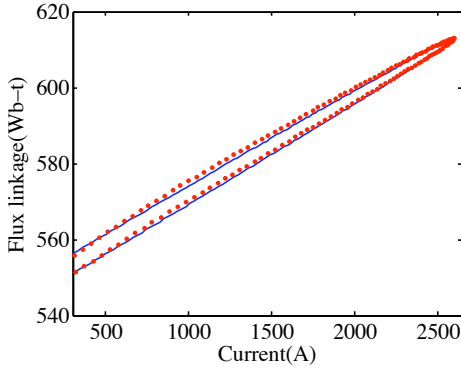


Fig. 12. Losses in the saturation region for the second benchmark using the A(x) model

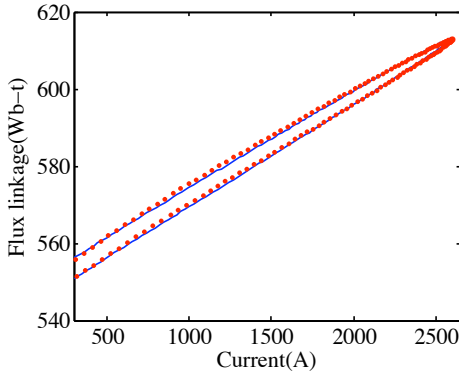


Fig. 13. Losses in the saturation region for the second benchmark using the EMTP-RV model

symmetrical, i.e. that the lower part of the ascending branch is a 180 degrees rotation of its upper part. However, this assumption is false, as it can be seen in Fig. 10, because of the wider area below saturation. On the other hand, the A(x) model is able to correctly reproduce these losses by using the whole upward branch for the curve fitting instead of just the upper part, not to mention that the A(x) function has more degrees of freedom than the hyperbolic function used in [7], which in turn implies that a better nonlinear regression can be achieved. Furthermore, the results from Fig. 12 and Fig. 13 show that both models can effectively reproduce the losses in the saturation region by means of the 950mΩ series resistance and with the correct saturation inductance level (slope), represented by parameter  $k_{13}$ .

## VI. CONCLUSIONS

A new modeling approach for the saturation and hysteresis phenomena was proposed and its implementation in the EMTP-RV solution method was presented. Two benchmarks were used for validation. The obtained results demonstrate that the model is adequate to reproduce the experimental data precisely. As a consequence, it was highlighted that in order to model the wider area near saturation, the branches cannot be symmetrical. Furthermore, the choice of the function to model this phenomenon is critical, in order to achieve a better nonlinear regression. In addition, since the trial and error fitting process with MATLAB is somewhat tedious, means of

automation to generate parameters  $k_1$  to  $k_{13}$  should be implemented in the future. Finally, since frequency dependency is desirable in some electromagnetic transient calculations, it is necessary to improve the model to account for the rate of change of magnetic flux.

## VII. APPENDIX

- A(x) model parameters for the first test:  $k_1 = 0.25$ ,  $k_2 = 1.5$ ,  $k_3 = 0.5$ ,  $k_4 = 0.0$ ,  $k_5 = 0.05$ ,  $k_6 = 0.3$ ,  $k_7 = 0.45$ ,  $k_8 = 0.0$ ,  $k_9 = 0.09$ ,  $k_{10} = 0.5$ ,  $k_{11} = 0.5$ ,  $k_{12} = 0.0$ ,  $k_{13} = 2 \cdot 10^{-3}$
- Simulation parameters for the first case: No initial conditions,  $t_{max} = 0.15s$ ,  $\Delta t = 1\mu s$
- A(x) model parameters for the second test:  $k_1 = 53.88$ ,  $k_2 = 0.01797$ ,  $k_3 = 0.0$ ,  $k_4 = 0.2001$ ,  $k_5 = 98.15$ ,  $k_6 = 0.2375$ ,  $k_7 = 0.7796$ ,  $k_8 = -0.126$ ,  $k_9 = 393.9$ ,  $k_{10} = 1.248$ ,  $k_{11} = 0.8129$ ,  $k_{12} = 0.4969$ ,  $k_{13} = 0.0257$
- EMTP-RV hysteretic reactor model parameters for the second test:  $S_{hv} = 4353.7$ ,  $S_{hh} = 54.21$ ,  $C_{hyst} = 95.49$ ,  $Coer = 1.085$ ,  $S_{sv} = 0.2883$ ,  $S_{sh} = 5.91 \cdot 10^{-6}$ ,  $C_{sat} = 944253.3$ ,  $Y_{sh} = 546.4$
- Simulation parameters for the second case: Steady-state initialization,  $t_{max} = 0.417s$ ,  $\Delta t = 10\mu s$

## VIII. REFERENCES

- [1] I. Mayergoyz, *Mathematical models of hysteresis and their applications*, 2nd ed. Elsevier, 2003.
- [2] G. Bertotti, *Hysteresis in magnetism*, 1st ed. Academic Press, 1998.
- [3] P. Langevin, "Magnétisme et théorie des électrons," *Ann. Chim. Phys.*, vol. V, pp. 70–127, 1905.
- [4] P. Weiss, "L'hypothèse du champ moléculaire et la propriété ferromagnétique," *J. de Phys. Radium*, vol. VI, pp. 661–690, 1907.
- [5] L. Brillouin, "Les moments de rotation et le magnétisme dans la mécanique ondulatoire," *J. de Phys. Radium*, vol. VIII, pp. 74–84, 1927.
- [6] S. Denetière, J. Mahseredjian, M. Martinez, M. Rioual, A. Xémard, and P. Bastard, "On the implementation of a hysteretic reactor model in EMTP," in *IPST-2003, International Conference on Power Systems Transients*, New Orleans, USA, September 2003.
- [7] A. Narang, E. P. Dick, and R. C. Cheung, "Transformer model for electromagnetic transient studies," Ontario Hydro Technologies, CEA Report No. 175 T 331G, December 1997.
- [8] J. Takács, *Mathematics of hysteretic phenomena*, 1st ed. Wiley VCH, 2003.
- [9] A. Rezaei-Zare, R. Iravani, M. Sanaye-Pasand, H. Mohseni, and S. Farhangi, "An accurate current transformer model based on Preisach theory for the analysis of electromagnetic transients," *IEEE Transactions on Power Delivery*, vol. 23, no. 1, pp. 233–242, Jan. 2008.
- [10] J. Mahseredjian, S. Denetière, L. Dubé, B. Khodabakhchian, and L. Gérin-Lajoie, "On a new approach for the simulation of transients in power systems," *Electric Power Systems Research*, vol. 77, no. 11, pp. 1514–1520, 2007.
- [11] J. Mahseredjian, *DLL programming, EMTP-RV documentation*, 2007.
- [12] S. Denetière, "Modélisation du phénomène d'hystérésis sous EMTP-RV," Master's thesis, École Polytechnique de Montréal, 2003.
- [13] MATLAB Curve Fitting Toolbox version 1.2, The MathWorks, Inc., 2007.
- [14] A. Gaudreau, P. Picher, L. Bolduc, and A. Coutu, "No-load losses in transformer under overexcitation/inrush-current conditions: Tests and a new model," *IEEE Transactions on Power Delivery*, vol. 17, no. 4, pp. 1009–1017, October 2002.
- [15] J. Frame, N. Mohan, and T.-H. Liu, "Hysteresis modeling in an electromagnetic transients program," *IEEE Transactions on Power Apparatus and Systems*, vol. PAS-101, no. 9, pp. 3403–3412, Sept. 1982.